4

THE HTTU TEST FACILITY

4.1 INTRODUCTION

Experimental test facilities aimed at measuring the effective thermal conductivity found in open literature are usually case specific and must be fully understood before any attempt can be made to compare simulation models with experimental data. This is particularly true when analysing the porous structure in each experimental setup. As mentioned previously, porosity alone cannot sufficiently characterise a packing structure in all the regions identified in Section 2.2.

In the extensive literature survey presented in Chapter 3, it was found that far more experimental research was conducted in the low temperature range with small diameter spheres than at high temperatures with larger spheres. Nonetheless some experimental investigations, apart from the newly built HTTU, were identified that could contribute to validate all the components of the newly proposed Multi-sphere Unit Cell Model, which is presented in Chapter 5. This experimental work is presented in Appendix C.

The HTTU actually forms part of a larger PBMR test facility. The purpose of this test facility is to provide data whereby advanced CFD modelling of different heat transfer and fluid flow phenomena may be validated through comprehensive separate effects tests and integrated effects tests. In the context of this study the results generated in the HTTU can be used to validate new models for the effective thermal conductivity via comparison between the empirical results and those provided by the models. Of specific interest to this study are the test results of the steady-state separate effects tests under near-vacuum conditions and at high temperatures.

The HTTU consists of two test section configurations namely a vacuum configuration and a forced flow configuration. The test section consists of a packed pebble bed with ± 28000 mono-sized 60 mm diameter graphite spheres inside an annular cylinder. The annular core has an outside diameter of 2.3 m and an inside diameter of 0.6 m. The height of the packed

bed is 1.2 m and a radial heat path is generated using graphite heater elements situated inside the inner reflector and a water jacket at the outer reflector, ensuring a near-uniform outer wall temperature. The schematic of the HTTU is displayed in Figure 4.1.

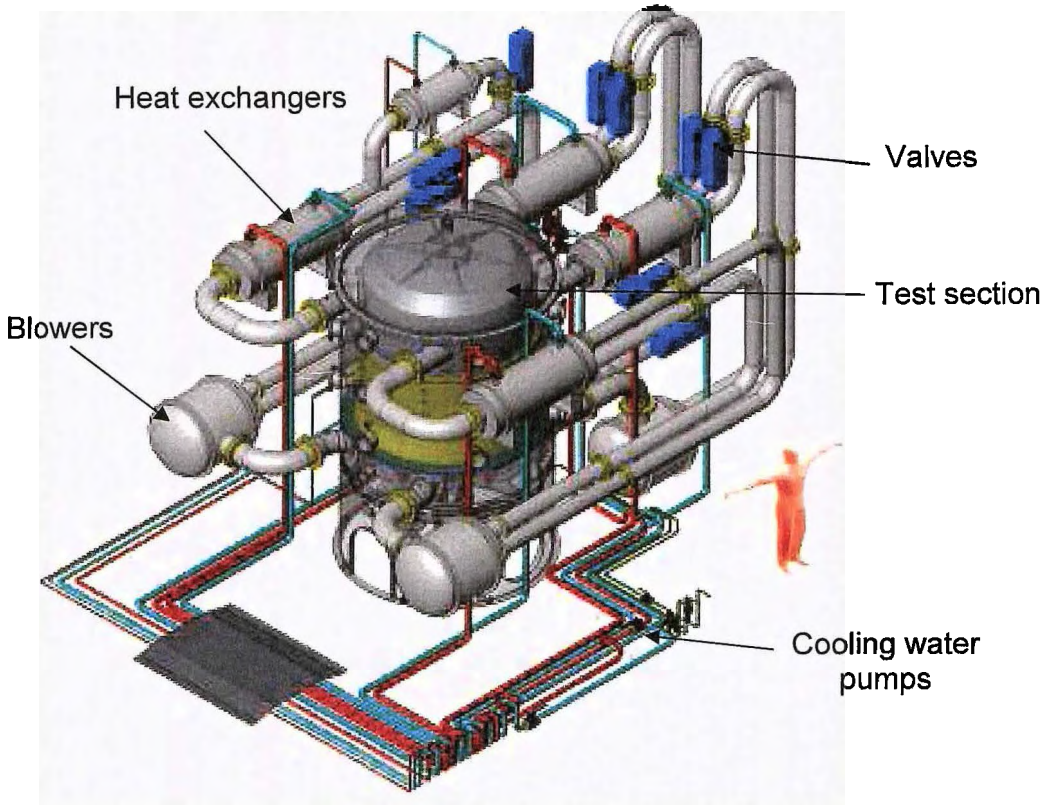

Figure 4.1: High Temperature Test Unit

4.2 PLANT CONFIGURATION

The HTTU vessel is a vertically orientated metal structure, designed to enclose all internals and provide flow nozzles to connect with process pipes. The vessel contains one removable top dome as main access into the vessel and four smaller access sites located at the bottom of the vessel as displayed in Figure 4.2.

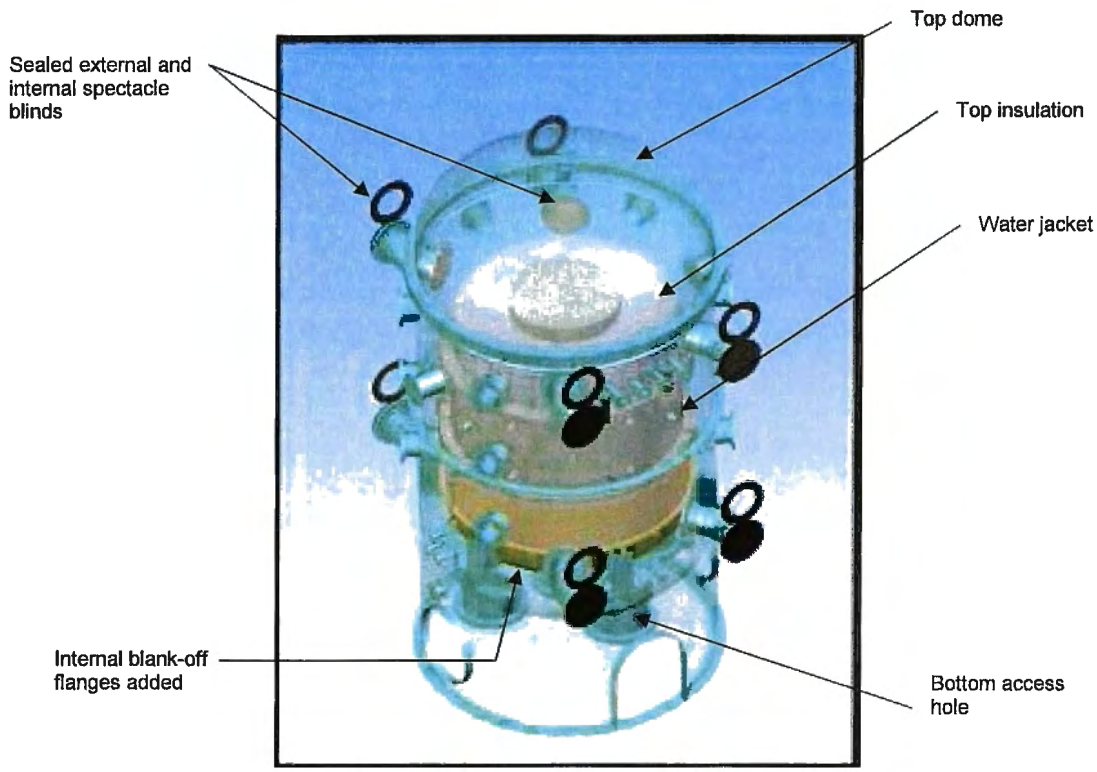

Figure 4.2: High Temperature Test Unit vessel (Van Antwerpen, W., 2009 (b):10)

Rousseau & Van Staden (2008:3060) stated that the purpose of the HTTU is amongst others to obtain detailed data with respect to the heat transfer phenomena in an annular packed bed. This is done in order to validate and, if necessary, improve the applicable correlations incorporated in the dynamic systems CFD code Flownex and the RANS CFD codes that are employed in the analysis and design of the PBMR power plant. The HTTU is a distorted model of a section of the PBMR, in order to limit the size and the cost of the facility. The distortion is with respect to the inner and outer radii of the annulus. However, the width of the annulus and the size of the spheres are the same. The inner and outer diameters of the HTTU annulus are 0.6 m and 2.3 m respectively, where the outer reflector is a cylindrical heat exchanger termed the water jacket.

Heat is generated within the HTTU by means of the graphite heater elements shown in Figure 4.5. Top and bottom insulation ensures minimal heat loss in the axial direction when heat is transported through the packed bed. The heat is then extracted through the water jacket at the outer wall. The water temperature at the inlet and outlet of the water jacket is held constant by automatically varying the water mass flow rate with a pneumatic valve.

The external and internal, top and bottom spectacle blinds are sealed off, ensuring an environment in which a constant system pressure of 10 kPa (absolute) can be maintained. Situated inside the graphite central column are several graphite heater elements connected to

a high electrical current with aluminium clamps. Small heat exchangers termed the stem coolers situated around these three main heater elements ensure that the electrical connections are operated at desirable temperatures at the various power inputs.

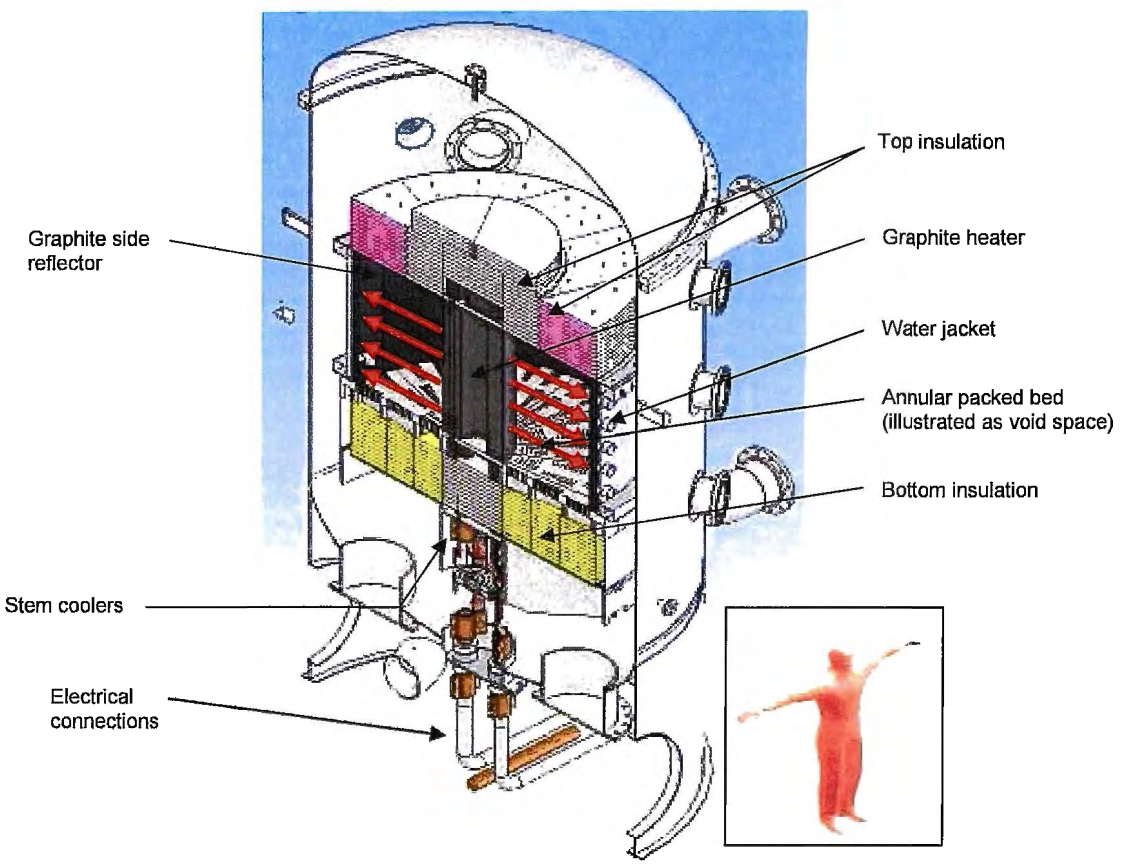

Figure 4.3: High Temperature Test Unit internals (Van Antwerpen, W., 2009 (b):10)

Figure 4.4: High Temperature Test Unit

Thermocouples are positioned at different (axial) levels in the annular randomly packed pebble bed, as illustrated in Figure 4.5. Each level consists of three different legs. The structured packing presented in Figure 4.5 is only for illustration purposes.

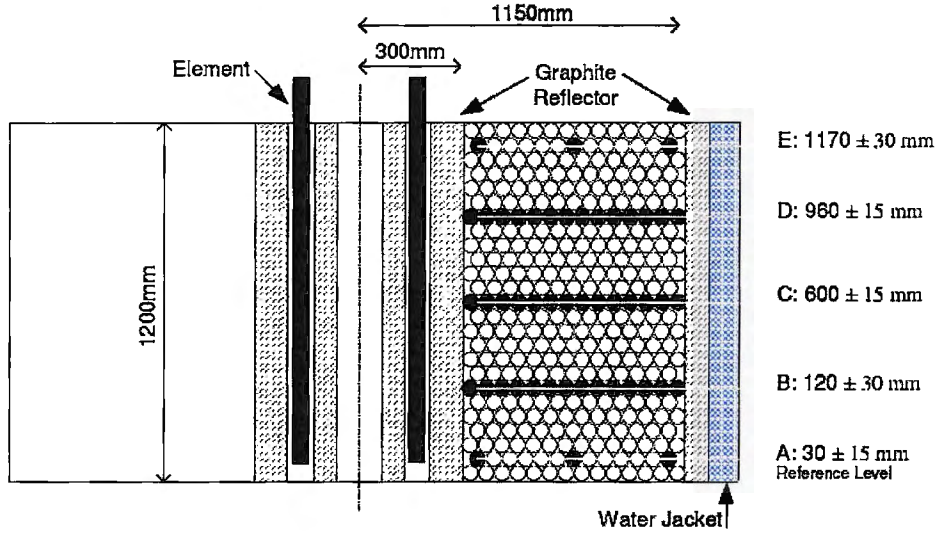

Figure 4.5: Thermocouple levels in the High Temperature Test Unit (Van Antwerpen, W., 2009 (b):10)

Levels A and E each consist of three thermocouples positioned in the centre of each graphite sphere, while levels B, C, D consist of eighteen thermocouples. In the case of levels B, C and D, two of the thermocouples are situated inside the inner graphite reflector, fourteen thermocouples are situated in the radial direction inside the pebble bed and two thermocouples are situated inside the outer graphite reflector. Tolerances were specified in the axial and radial direction for each level owing to the randomness of the packed bed. The

packed bed is further divided into three different heat zones. In each heat zone, a different type of thermocouples is used due to the cost implication, as illustrated in Figure 4.6.

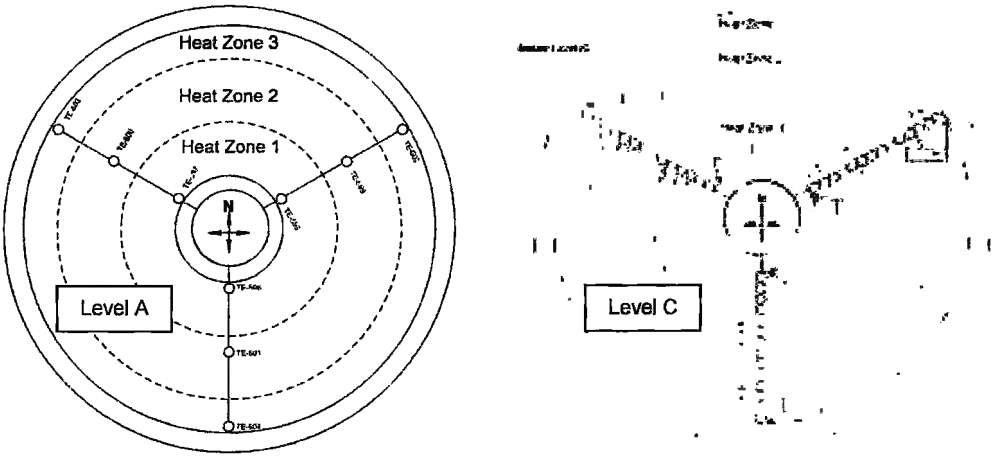

Figure 4.6: Thermocouple levels in the High Temperature Test Unit (Van Antwerpen, W., 2009 (b):10)

4.3 TEST MATRIX

Two full-scale Nitrogen High Temperature Near-Vacuum tests were conducted in order to ensure that the experimental results obtained could be repeated in further studies. The test schedule for a particular test was according to the test matrix presented in Figure 4.7.

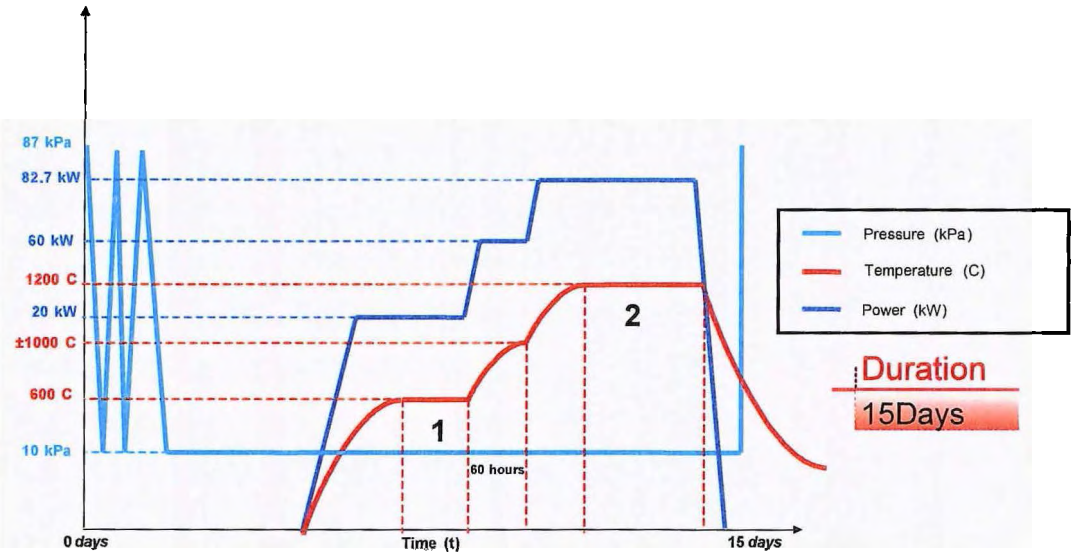

Figure 4.7: Test matrix for Nitrogen High Temperature Near-Vacuum tests (Van Antwerpen, W., 2009 (b):10)

In Figure 4.7, it is indicated that test results were generated from a sixty-hour transient and two steady-state tests namely 1 and 2. Because a rate limiter was installed to protect the

heater from a sudden increase in amperage, the power increase is not a vertical step. A power step would have taken more or less eight minutes depending on the magnitude of the step. However, the heat capacity of the system is so large that the influence of the rate limiter on the system is negligible. It should also be noted that ambient temperatures and pressures are not reported because they are not applicable in this analysis.

4.4 DERIVATION OF THE EFFECTIVE THERMAL CONDUCTIVITY FROM THE EXPERIMENTAL DATA

A set of radial temperature profiles for each axial level and radial leg were obtained for each steady-state condition achieved. The stem coolers situated at the bottom of the packed bed influenced the detailed temperature measurements at level B as was predicted during the design analysis. The radial temperature profiles obtained from level C and D closely matched each other. Therefore, it was decided to use the detailed radial temperature profiles of level C. Looking at the isothermal temperature distribution in the axial direction, presented in Figure 4.8, it can be concluded that level C is a viable option for the derivation of the effective thermal conductivity, due to the small impact of the stem coolers. The temperature profiles for both tests are displayed in Figure D.4 and Figure D.5.

Using these radial temperature profile measurements, the effective thermal conductivity k_{eff} can be derived using Fourier's Law given as:

$$Q_{bed} = -k_{eff} 2\pi r L \frac{dT}{dr} \tag{4.1}$$

Eq. (4.1) can be rewritten to become:

$$k_{eff} = \frac{-Q_{bed}}{2\pi r L\, dT/dr} \tag{4.2}$$

where $Q_{bed} = Q_{bed}(r)$ is the effective heat flux transported through the packed bed as a function of radial position due to the axial heat losses through the top and bottom insulation, $L = 1.2m$ and dT/dr the slope (derivative) of the temperature profile. In order to determine the heat loss in the axial direction through the top and bottom insulation, it was assumed that the isotherms were perfectly vertical, which lead to a known radial temperature distribution on the inner surfaces of the top and bottom insulation. Therefore, a certain amount of heat was lost through the top and bottom insulation of the HTTU, indicated with $Q_{i,loss}(r)$ and varied with radial position owing to the variation in the temperature and the transport area through the insulation.

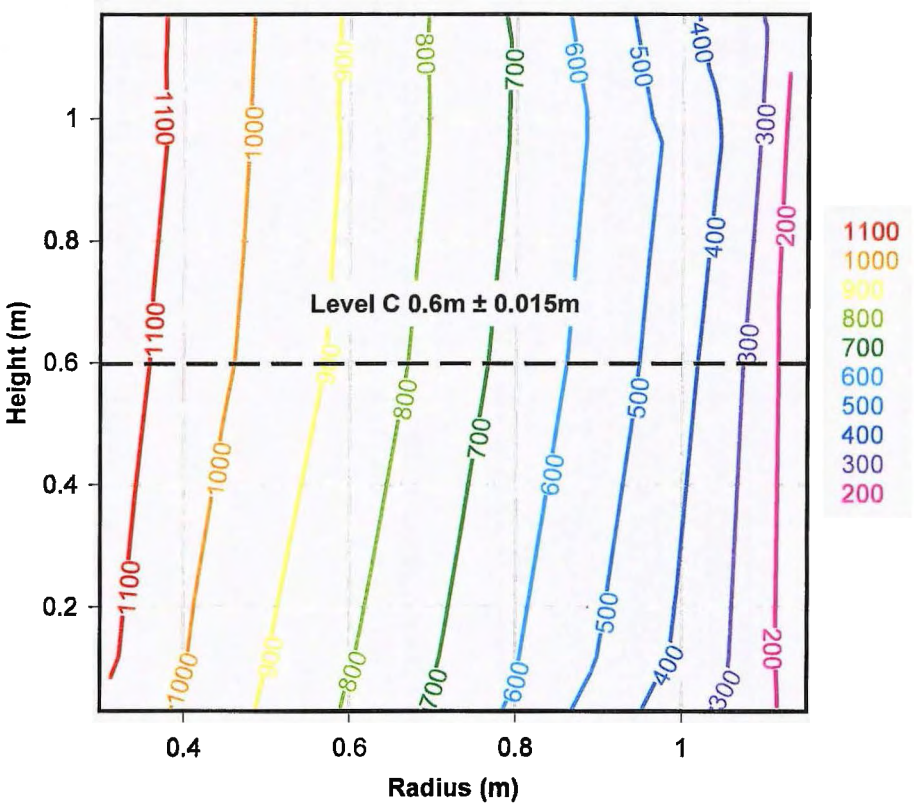

Figure 4.8: Isothermal temperature distribution (1200°C steady-state)

The heat loss through the insulation was incorporated by discretising the top and bottom insulation into forty equally spaced radial increments. An illustration for the top insulation is given in Figure D.1 (Appendix D). For each increment, the heat loss was calculated as follows:

$$Q_{i,loss} = \frac{k_{ins} A_i}{L_{ins}} \left(T_{bed} - T_{env}\right) \tag{4.3}$$

where k_{ins} is the insulation thermal conductivity, L_{ins} the insulation height, T_{env} the environmental temperature and $A_i = 2\pi\left(r_{i+1}^2 - r_i^2\right)$ the conduction area. The full analysis in the derivation of Q_{bed} can be found in Appendix D and in Van Antwerpen, W. (2009 (b):1).

Van Antwerpen, H.J. (2009:12) illustrated that a least squares fit of a higher-order polynomial to the temperature measurements of each test can be used in order to calculate the temperature gradient (slope) dT/dr for extraction of effective thermal conductivity in the HTTU. Unweighted linear least-squares regression was used as described in Appendix D. It is termed "linear", as the regression function is linear with regards to the coefficients of the regression function (the polynomial). Therefore, it is possible to solve the coefficient values directly from a system of linear independent equations to obtain the least-squares solution to the regression optimisation problem.

The matrix-vector equation solution functions of Microsoft Excel were used to calculate the regression function coefficients. This approach also enabled quick changes in the polynomial order. A fifth-order polynomial was found to give the best results in terms of the cumulative uncertainty. The regression function was differentiated analytically to obtain the temperature gradient as function of position.

4.5 UNCERTAINTY ANALYSIS

In general, an uncertainty implies a parameter associated with the result of a measurement, or the combined result of several measurements, that characterises the dispersion or the width of a specific confidence interval. There are three different types of uncertainties that are considered to contribute to the total uncertainty in the HTTU i.e. statistical variance, instrument uncertainty and drift uncertainty.

To calculate the statistical variance the following procedure is used:

$$u\left(x_{i,statistical}\right)=\sqrt{\frac{\sum_{i=1}^{N}\left(x_i-\bar{x}\right)^2}{N}} \tag{4.4}$$

where x_i is the measured temperature value and $\bar{x}$ the average of the N sample points. The instrument uncertainty $u\left(x_{i,instrument}\right)$ on the other hand is obtained from the manufacturer and the drift uncertainty $u\left(x_{i,drift}\right)$ after each major calibration. The uncertainties are then combined to give a total standard uncertainty employing the following formula:

$$u\left(x_{i,\exp}\right)=\sqrt{\left[u\left(x_{i,statistical}\right)\right]^2+\left[u\left(x_{i,instrument}\right)\right]^2+\left[u\left(x_{i,drift}\right)\right]^2} \tag{4.5}$$

Van Antwerpen, W. (2009 (b):17) derived the equation to obtain the uncertainty in k_{eff} presented in Eq. (4.6) with the respective partial derivatives shown in Eq. (4.7) and Eq. (4.8).

$$u\left(k_{eff}\right)=\sqrt{\left[\frac{\partial\left(k_{eff}\right)}{\partial Q_{bed}}\cdot u\left(Q_{bed}\right)\right]^2+\left[\frac{\partial\left(k_{eff}\right)}{\partial\left(dT/dr\right)}\cdot u\left(dT/dr\right)\right]^2} \tag{4.6}$$

$$\frac{\partial\left(k_{eff}\right)}{\partial Q_{bed}}=\frac{-1}{2\pi rL\,dT/dr} \tag{4.7}$$

$$\frac{\partial\left(k_{eff}\right)}{\partial\left(dT/dr\right)}=\frac{Q_{bed}}{2\pi rL\left(dT/dr\right)^2} \tag{4.8}$$

The uncertainty analysis with the final effective thermal conductivity values for both steady-state tests are shown in Appendix D and can also be seen in Van Antwerpen, H.J. (2009:1). Calculation results revealed that the uncertainty in all cases is the highest at the inner wall region, where the temperature is the highest. The maximum uncertainty was found to be 11.4% on effective thermal conductivity for the 20kW steady-state tests at the inner reflector, where for the 1200°C steady-state the maximum uncertainty on effective thermal conductivity was found to be 8.6% at the inner reflector.

4.6 EXPERIMENTAL RESULTS

In the general thermal fluid community effective thermal conductivity is always represented as a function of temperature as displayed in Figure 4.9 for the HTTU effective thermal conductivity results. However, using this methodology the wall effects cannot be pinpointed to a specific radial position in the packed bed. Therefore, wall effects are better illustrated plotting effective thermal conductivity as a function of sphere diameter from the inner wall as shown in Figure 4.10.

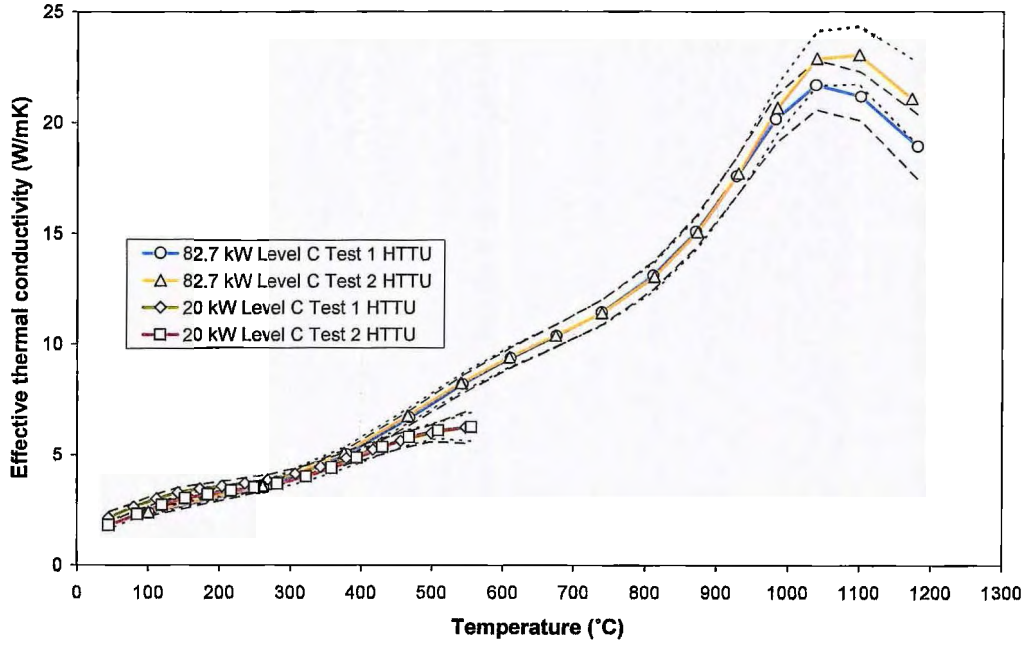

Figure 4.9: HTTU experimental results effective thermal conductivity against temperature level C (1200°C steady-state)

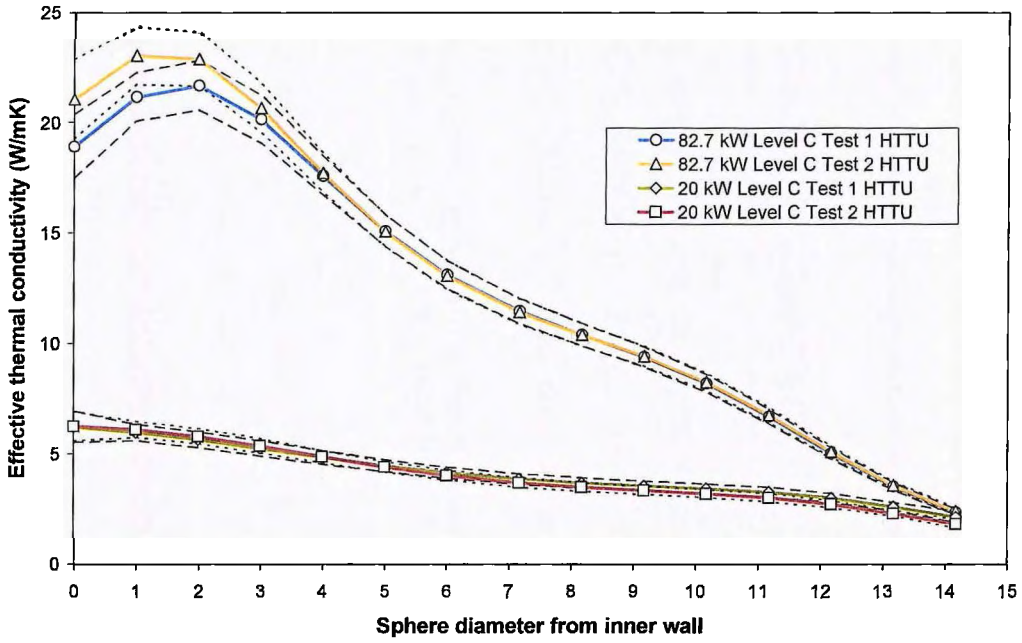

Figure 4.10: HTTU experimental results effective thermal conductivity against sphere diameter from inner wall level C (1200°C steady-state)

4.7 CONCLUSION

A description of the HTTU has been presented in this chapter. The method employed to quantify the axial heat loss through the top and bottom insulation in the determination of the effective thermal conductivities at two different steady-states was also presented. The effective thermal conductivity results were extracted using a polynomial method and an uncertainty analysis was conducted in order to determine the confidence interval of the experimental results.